Modelling motor cortex stimulation for chronic pain control: electrical potential field, activating functions and responses of simple nerve fibre models

L. Manola[1] B. H. Roelofsen[1] J. Holsheimer[1] E. Marani[1,2] J. Geelen[1,3]

[1]Institute for Biomedical Technology, University of Twente, Enschede, The Netherlands
[2]Neuroregulation Group, Department of Neurosurgery, Leiden University Medical Centre, Leiden, The Netherlands
[3]Department of Neurology, Medical Spectrum Twente Hospital, Enschede, The Netherlands

Abstract—*This computer modelling study on motor cortex stimulation (MCS) introduced a motor cortex model, developed to calculate the imposed electrical potential field characteristics and the initial response of simple fibre models to stimulation of the precentral gyrus by an epidural electrode, as applied in the treatment of chronic, intractable pain. The model consisted of two parts: a three-dimensional volume conductor based on tissue conductivities and human anatomical data, in which the stimulation-induced potential field was computed, and myelinated nerve fibre models allowing the calculation of their response to this field. A simple afferent fibre branch and three simple efferent fibres leaving the cortex at different positions in the precentral gyrus were implemented. It was shown that the thickness of the cerebrospinal fluid (CSF) layer between the dura mater and the cortex below the stimulating electrode substantially affected the distribution of the electrical potential field in the precentral gyrus and thus the threshold stimulus for motor responses and the therapeutic stimulation amplitude. When the CSF thickness was increased from 0 to 2.5 mm, the load impedance decreased by 28%, and the stimulation amplitude increased by 6.6 V for each millimetre of CSF. Owing to the large anode–cathode distance (10 mm centre-to-centre) in MCS, the cathodal fields in mono- and bipolar stimulation were almost identical. Calculation of activating functions and fibre responses showed that only nerve fibres with a directional component parallel to the electrode surface were excitable by a cathode, whereas fibres perpendicular to the electrode surface were excitable under an anode.*

Keywords—*Motor cortex stimulation, Chronic pain, Volume conductor model, Nerve fibre model, Activating function*

Med. Biol. Eng. Comput., 2005, **43**, 335–343

1 Introduction

1.1 *General introduction*

MOTOR CORTEX stimulation (MCS) has been applied in the last 12 years as a treatment for several types of chronic, intractable pain. Nearly 300 cases of MCS have been published. Although the clinical results are variable, the number of published cases in which MCS was applied successfully in the treatment of central post stroke pain (CPSP) and trigeminal neuralgia (TGN) allows the conclusion that these indications are validated for MCS treatment (BROWN and BARBARO, 2003).

In MCS, an electrode is placed epidurally over the location on the precentral gyrus where the contralateral painful body area is represented. The surgical procedure has been described by for example, GARCIA-LARREA *et al.* (1999) and NGUYEN *et al.* (2000). Neurophysiological stimulus-response methods and advanced neuro-navigation techniques support the precise placement of the stimulating electrode, reported to be critical for successful MCS (NGUYEN *et al.*, 1999; PIROTTE *et al.*, 2001).

As a first step to unravelling the analgesic mechanism of MCS, PET scans have been performed after implantation (GARCIA-LARREA *et al.*, 1999). The most significant increase in regional cerebral blood flow, which corresponds to an increase in metabolism as a result of increased neuronal activity, has been observed in the ventro-anterior (VA) and the ventro-lateral (VL) nuclei of the thalamus.

The aim of this study was to predict the immediate bioelectrical effects of MCS by computer modelling. Apart from analysis of the stimulation-induced field, this study also aims to explore the resulting response of simple fibre models in the precentral gyrus. More sophisticated fibre models are still being developed.

Correspondence should be addressed to Dr Jan Holsheimer; email: j.holsheimer@el.utwente.nl

Paper received 22 November 2004 and in final form 8 December 2004

MBEC online number: 20053991

1.2 *Anatomical aspects*

The brain surface is covered by membranes that enclose the cerebrospinal fluid. The inner membrane, or pia mater, covers the cortical surface completely, including the various sulci and fissures. It is connected by thin filaments to the arachnoid, forming the middle membrane. The outer and thickest membrane, the dura mater, is covered by a thin layer of epidural fat and follows the bony structure of the skull.

At the pial surface, the precentral gyrus is situated between the central sulcus and the precentral sulcus, on its posterior and anterior sides, respectively. The lateral fissure and, at the interhemispheric side, the sulcus cinguli form its inferior and superior anatomical borders, respectively (NIEUWENHUYS *et al.*, 1988).

The primary motor cortex comprises of a thin layer of grey matter and its afferent and efferent fibres in the white matter beneath. The primary motor cortex (Brodmann's area 4), which is characterised by the presence of the giant cells of Betz, partly covers the precentral gyrus. Near the lateral fissure, it is practically limited to the anterior wall of the central sulcus. Superiorly, the primary motor cortex increasingly widens and covers the whole convexity of the precentral gyrus at its border with the interhemispheric fissure. The complementary part of the precentral gyrus is covered by the premotor cortex or Brodmann's area 6 (see ZILLES (1990)). Both the primary and the premotor cortices have a somatotopic organisation. The face is represented most inferiorly, and the lower extremities project to the superior area of the precentral gyrus, which extends into the wall of the interhemispheric fissure (TRUEX and CARPENTER, 1964; ZEFFIRO, 1990).

The motor cortex has a laminated structure of six layers, as shown in Fig. 1*a*. In this Figure cell bodies, dendrites and axons are made visible by different staining methods. The main inputs of the motor cortex originate from the cerebellum and the pallidum by the VA and VL nuclei of the thalamus. The ramifications of these thalamocortical fibres constitute parts of the 'horizontal' sheets of myelinated fibres, primarily in layer IV of the motor cortex (ZILLES, 1990). Corticothalamic neurons in layers V and VI project to the VA–VL complex, thus closing the corticothalamic loop (NA *et al.*, 1997; OHYE, 1990).

No data were found in the literature on the distribution of nerve fibre diameters in the various layers of the motor cortex. In particular, the largest fibres in each afferent and efferent pathway are of interest, because these fibres need the lowest stimulus for their excitation. The largest fibre diameter measured in a study on human brain white matter (not including the axons of Betz cells) is 4 μm (TANG and NYENGAARD, 1997). Some Betz cell efferents are among the largest fibres in the pyramidal tract and can have diameters up to 13 μm (GRAF VON KEYSERLINGK and SCHRAM, 1984; TRUEX and CARPENTER, 1964). As the mean size of Betz cells (in layer V) is larger in the superior part (limbs) than in the inferior part (face) of the precentral gyrus, it is likely that the mean calibre of their efferents is also larger in the superior part.

All pyramidal cells have a long apical dendritic tree perpendicular to the cortical layers and extending into layer I. Their efferents have the same orientation with respect to the cortical layers, thus creating a 'fountain' of nerve fibres emerging from the white matter into the grey matter of the precentral gyrus, as shown in Fig. 1*b* (see also VILLIGER (1940)).

2 Methods

2.1 *Volume conductor model*

2.1.1 *Geometry*

A 3D, inhomogeneous and partly anisotropic volume conductor model, representing the grey and white matter of the precentral gyrus, as well as the surrounding anatomical structures, has been constructed. Fig. 2 shows a transverse cross-section of this 3D model that represents part of the gyrus, with the precentral and central sulci on the left and right sides, respectively. The 80 layers that compose the model from inferior to superior (z-direction) have the same geometry, except for the outer ones, which are used as boundary layers. Each layer consists of 6300 cubic elements, each defined by an (an)isotropic conductivity. The length of the rib of a cube was chosen to be smallest (0.3 mm) in the vicinity of the epidural electrode, where the voltage gradient is largest.

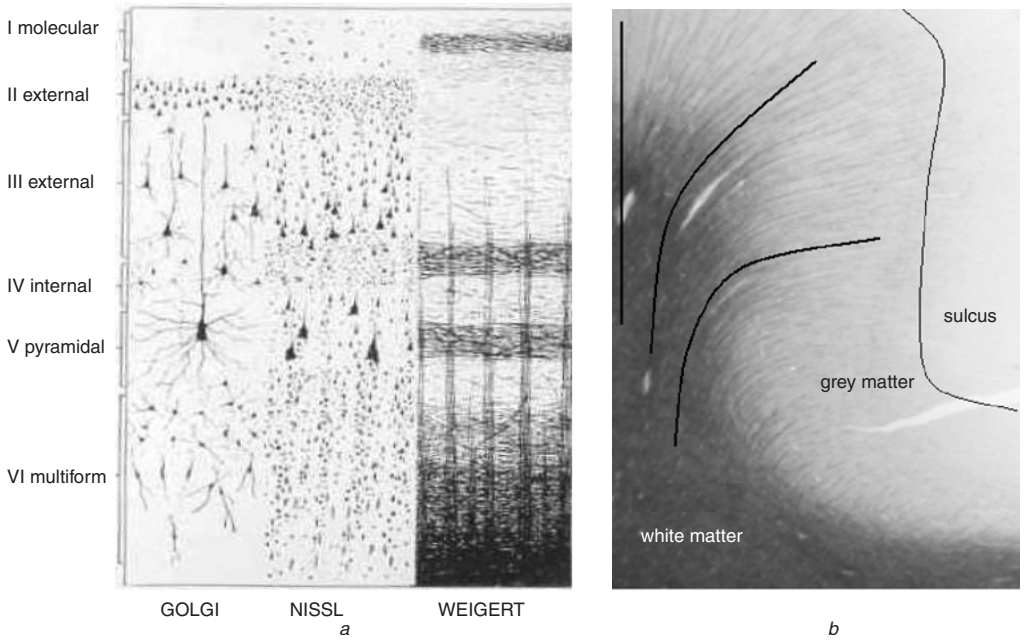

Fig. 1 *(a) Layered structure of motor cortex (laminae I–VI); cortical afferents from various parts of brain ascend and bifurcate into specific layer parallel to cortical surface; giant cells of Betz are located in layer V; (b) efferents of pyramidal neurons leave cortex into white matter below, creating 'fountain' of fibres in gyrus*

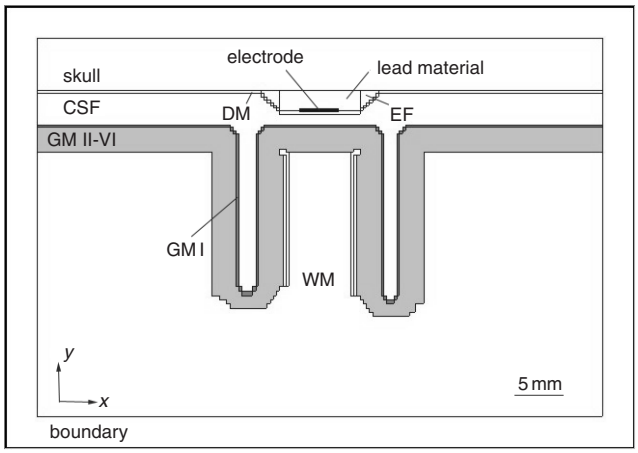

Fig. 2 *Transverse section (xy-plane) of 3D volume conductor model through centre of epidural electrode;* ***Dm****-dura mater;* ***CSF****-cerebrospinal fluid;* ***EF****-epidural fat,* ***GM I****: cortical layer I;* ***GM II–VI****: layers II–VI*

The implanted stimulating device was modelled according to the dimensions of the paddle of a Resume II lead* generally used in MCS: a 2 mm thick, 8 mm wide and 44 mm long insulator. This paddle model was placed between the skull and the dura mater from inferior to superior above the precentral gyrus. Each metal electrode was a disc with a diameter of 4 mm on the lower side of the paddle, directly above the dura mater. To model monopolar or bipolar stimulation, one electrode, or two electrodes at a centre-to-centre distance of 10 mm on the paddle, were defined.

The dimensions of the model in the x-, y- and z-directions were 60.8 × 42.6 × 57.4 mm, respectively. Table 1 presents an overview of the geometries of the modelled anatomical compartments. The arachnoid and the pia mater were not incorporated in the model as separate compartments.

2.1.2 *Conductivities*

The electrical conductivities of the anatomical model compartments are presented in Table 2. The conductivities of most compartments were taken from the spinal cord stimulation model developed in our group. The conductivity of the grey matter, however, was inhomogeneous, with layer I having a ∼60% lower value than layers II–VI. This value was estimated from empirical data by HABERLY and SHEPHERD (1973) and HOELTZELL and DYKES (1979). In both studies, a large gradient in conductivity was reported from layer I to layer II. The conductivity of the white matter was anisotropic, having the higher value in the direction of the myelinated fibres.

The conductivity of the boundary layer, representing distant tissues, was chosen such that the model impedance matched the mean empirical value for monopolar stimulation (∼750 Ω). The conductivity of the dura mater was given a value at which the model impedance matched the mean empirical value in bipolar stimulation (∼1000 Ω).

2.1.3 *Computation of 3D potential field*

A finite difference method was implemented in the simulation software to solve the potentials at the grid-points of the model resulting from the voltage(s) allocated to the electrode(s). These grid-points were the vertices of the cubic elements forming the volume conductor model. For each volume element, conservation of charge applies, as expressed by

$$\nabla \cdot \boldsymbol{J}^{total} = 0 \tag{1}$$

*Medtronic Inc., Minneapolis, MN, USA

The total current density $\boldsymbol{J}^{total}$ includes a conduction current density and an impressed current density. The latter arises from bioelectric sources within the tissue. In the MCS model, the assumption is made that bioelectrical sources have a negligible influence on the stimulation induced electrical field. Therefore only the conduction current density is left, which can be written as the product of the conductivity vector σ and the electrical field vector $\boldsymbol{E}$

$$\boldsymbol{J}^{total} = \sigma \boldsymbol{E} \tag{2}$$

with $\boldsymbol{E}$ expressed as the negative gradient of the potential field

$$\boldsymbol{J}^{total} = -\sigma \nabla \Phi \tag{3}$$

Substitution of (3) into (1) yields the Laplace equation of the potential field

$$\nabla \cdot \sigma \nabla \Phi = 0 \tag{4}$$

The boundary conditions applied are of the Dirichlet type: at the electrode surface: Φ = constant; at the model surface: $\Phi = 0$.

Taylor's theorem was utilised to provide the finite difference representation of (4) in which the potentials at the individual grid-points appear. Thus a second-order approximation of the equation for the potential at grid-point (x,y,z) with a homogeneous medium and a uniform grid becomes

$$\begin{aligned} &\sigma_x \frac{\Phi_{x-1,y,z} - 2\Phi_{x,y,z} + \Phi_{x+1,y,z}}{(\Delta x)^2} \\ &+ \sigma_y \frac{\Phi_{x,y-1,z} - 2\Phi_{x,y,z} + \Phi_{x,y+1,z}}{(\Delta y)^2} \\ &+ \sigma_z \frac{\Phi_{x,y,z-1} - 2\Phi_{x,y,z} + \Phi_{x,y,z+1}}{(\Delta z)^2} = 0 \end{aligned} \tag{5}$$

Each of the three terms of (5) belongs to an orthogonal direction. The square of the local resolution is the denominator of each term. Each nominator contains the appropriate conductivity vector component and the potentials at three successive grid-points along an axis. The equations for all grid-points in the model constitute the linear system

$$\boldsymbol{A}\Phi = \boldsymbol{b} \tag{6}$$

in which matrix $\boldsymbol{A}$ contains the grid spacing and vertex conductivity information, Φ contains the potentials at the non-boundary grid-points, and $\boldsymbol{b}$ contains the information about the Dirichlet conditions.

The matrix equation (6) was solved for the potentials at the grid-points according to the red–black Gauss–Seidel algorithm with variable over-relaxation. To obtain a reliable solution, the procedure was implemented in such a way that two independent iterations with different initial guesses of $\boldsymbol{\Phi}$ converge to the final solution. The stopping criterion was defined as

$$\frac{\sum_{i=1}^{n} |\Phi_i' - \Phi_i''|}{n} < 0.0001\ \mathrm{V} \tag{7}$$

where Φ_i' and Φ_i'' are the potentials on grid-point i calculated by each iteration procedure, and n is the number of grid-points of the model.

Table 1 Human anatomical data implemented in MCS model

Parameter	Mean, mm	SD, mm	*n*	Reference(s)
Skull thickness (over motor cortex)	5		93	VAN VEENENDAAL (1982) (unpublished)
Dura mater thickness	0.36		>100	MCCOMB *et al.* (1981), JIANG (1990)
CSF layer thickness (over precentral cortex)	3.1	0.8	6	ROELOFSEN, (2003) (unpublished) (T2 weighted MRI density profiles)
Motor cortex thickness layer I	0.2			ZILLES (1990) (Brodmann area 4)
layers II–IV	1.4			
layers V–VI	2.1			
Precentral gyrus width	11.7	4.9		ROELOFSEN (2003) (unpublished) (all parameters measured at 5 positions along precentral gyrus of 6 fixated hemispheres; corrected for 15% shrinkage)
Central sulcus width	2.7	0.73		
Precentral sulcus width	2.3	1.1		
Central sulcus depth	16.4	4.0		
Precentral sulcus depth	15.6	4.0		

2.2 *Nerve fibre model*

A McNeal-type cable model (MCNEAL, 1976) with sealed ends (infinite termination impedance) was incorporated in the simulation software to predict the response of myelinated nerve fibres to the external potential field. All nodes of Ranvier of the fibre were made excitable, having modified Frankenhaeuser–Huxley membrane kinetics adjusted to experimental data of human sensory fibres at 37°C. The internodal portion of the fibre membrane was assumed to be an ideal insulator. For a detailed description of the fibre model, see WESSELINK *et al.* (1999).

Four fibre types were modelled, as shown in Fig. 3. All fibre models were placed in the transverse cross-section (*xy*-plane) through the centre of the electrode (Fig. 2). The course of fibre model A_1 is parallel to the cortical surface at a depth of 1.4 mm and represents a thalamocortical (afferent) fibre branch in layer IV. Fibre models E_1–E_3 represent cortical efferents arising in layer V, with orientations based on their course in the cortex and the white matter below, as depicted in Fig. 1*b*.

According to the inverse recruitment principle, the threshold stimulus of a fibre group is related to the excitation of the largest fibres in this group. To obtain the threshold stimuli of the efferent fibre groups represented by fibre models E_1–E_3, these fibre models should be considered as efferents of the giant cells of Betz in layer V that project into the corticofugal motor system. Based on neuro-anatomical studies (see Section 1.2), it is assumed that these axons have a diameter exceeding the size of the efferents projecting from laminae V and VI to the VA–VL complex of the thalamus.

Each efferent fibre model E_1–E_3 originates in layer V and leaves the cortex at a different location, thus resulting in different orientations of the initial parts of these fibre models. Fibre model E_1 originates in the convexity of the precentral gyrus, and its course is perpendicular to the electrode surface. Fibre model E_2 originates at a location where the cortex bends from a horizontal to a vertical orientation, forming the anterior wall of the central sulcus. The initial part of this fibre model is at an angle of 45° to the electrode surface. Fibre model E_3 leaves the cortex deeper in the anterior wall of the central sulcus, and the orientation of its initial part is parallel to the electrode surface. Note that fibre type E_1 is only present in the superior region of the precentral gyrus, where Brodmann area 4 extends over the convexity of the gyrus (see Section 1.2).

Table 2 Conductivities in MCS model

Compartment	Conductivity, $S(m)^{-1}$
Skull	0.02
Epidural fat (**EF**)	0.04
Lead material	0.0001
Dura mater (**DM**)	0.065
Cerebrospinal fluid (**CSF**)	1.7
Grey matter	
layer I (**GM I**)	0.14
layer II–VI (**GM II–VI**)	0.36
White matter	
parallel to fibres	0.6
perpendicular to fibres	0.083
Boundary layer	0.0009

3 Results

3.1 *Influence of the grid on the calculated electrical potential field*

The total grid size (number of grid-points) and the grid spacing in each orthogonal direction of the model were chosen such that all anatomical structures could be represented

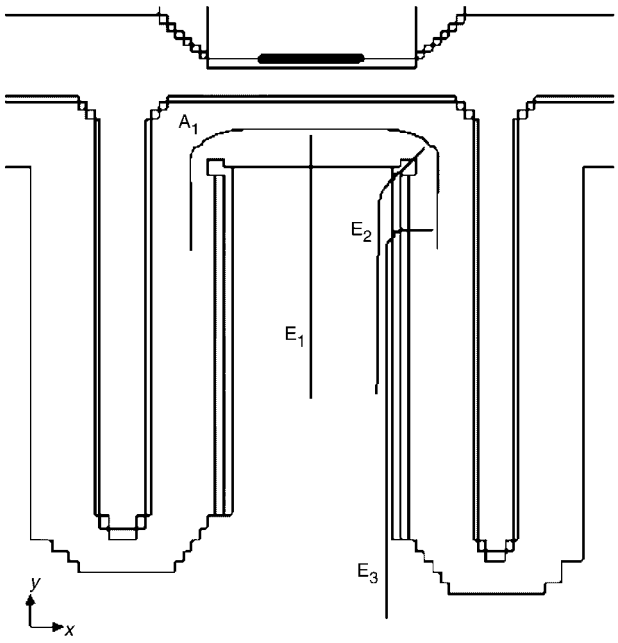

Fig. 3 *Cortical fibre models:* ***A*****$_1$***: 'horizontal' branch of cortical afferent at depth of 1.4 mm in cortex;* ***E*****$_1$**–**E_3***: cortical efferents of Betz cells in layer V, leaving cortex at different locations in gyrus*

with a satisfactory resolution, while the computational load, which is a power function of the total number of grid-points, was limited. To test how sensitive the calculated electrical potential field was to the chosen grid, the grid was refined twice in all three directions. For calculation with the finer grid, the iterative Gauss–Seidel procedure was stopped when the average final residuals of the discrete equation were four times less than those obtained with the coarser grid, which took ~16 times longer to accomplish.

The two field solutions resulted in a small mean difference (<2.5%) and a maximum of about 10% only around the edge of the electrode. However, this was not considered to be relevant, as the neural structures to be stimulated were far more distant from the electrode. Indeed, model output parameters, such as fibre model thresholds and the lumped tissue impedance, differed by less than 3% (and all had a deflection of the same sign).

Based on these sensitivity tests, we concluded that the original model with $91 \times 71 \times 81$ grid-points provided a sufficiently accurate solution obtained within a reasonable computation time (~4000 iterations and 60–90 min, depending on the PC). All results presented were calculated with this model.

3.2 *Cathodal field at monopolar and bipolar stimulation*

As MCS is applied both monopolarly and bipolarly, we compared the corresponding fields in the precentral gyrus. To eliminate the effect of different load impedances in mono- and bipolar stimulation, a 1 mA current was applied in both cases, and each stimulation-induced field was represented by an identical set of ten iso–current density lines in a plane parallel to the surface of the electrode(s) and at a depth of 1.4 mm in the cortex.

As shown in Fig. 4, the current density field is circular for monopolar stimulation. For bipolar stimulation, the symmetry in the *x*-direction is maintained, but the current density field is slightly more confined towards the axis of the bipole. In the *z*-direction, the outtermost iso-lines of the bipolar field (representing the lowest current densities) extend more towards the other pole, whereas the iso-lines representing higher current densities are still circular, virtually creating a monopolar current-density field.

3.3 *Sensitivity of the current density field to the width of the sulci*

The widths of the precentral and central sulci had a standard deviation of 41% and 30% of the corresponding mean values (see Table 1). To investigate the influence of this variability on the current-density field in the cortex below an electrode, models were made in which the average width of each sulcus was increased by the standard deviation. The current density field was quantified by calculation of the average of the normal current-density component in two *yz*-planes in the cortex, situated on the edges of the electrode (see Fig. 2). Stimulation was applied monopolarly (−1 V).

On the side of the precentral sulcus, the average normal current-density component in the cortical *yz*-plane was 1.3% higher as a result of a 41% wider precentral sulcus. Similarly, a 30% wider central sulcus resulted in a 1.0% increase of the average normal current density component in the cortical *yz*-plane on the side of the central sulcus.

3.4 *Influence of the CSF layer below the electrode on the current-density field*

In Figs 5*a* and *b*, iso-current density lines are depicted in a transverse (*xy*) and a longitudinal (*yz*) plane through the centre of the electrode in monopolar (cathodal) stimulation.

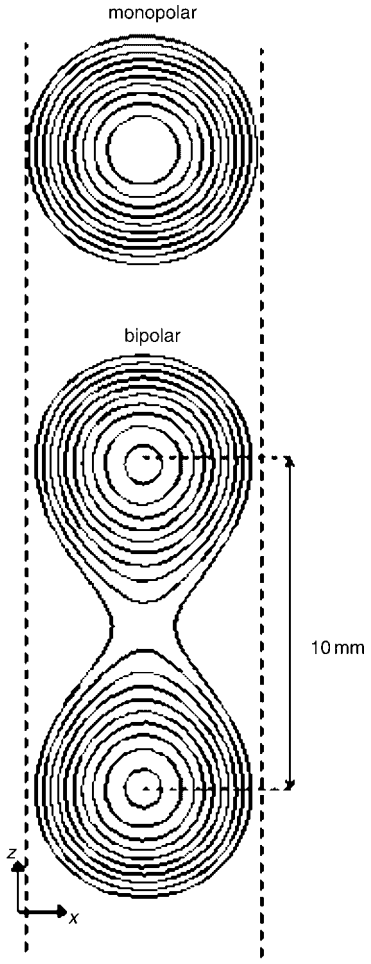

Fig. 4 *Iso-current density lines in xz-plane of model parallel to electrode surface(s) at depth of 1.4 mm in cortex; ten equidistant lines (4.5–7.5 μA mm^{-2}); mono- and bipolar stimulation (1 mA)*

Owing to the inhomogeneous medium, the iso-lines are not circular around the electrode (as would be expected in a homogeneous medium). The highest current densities are in the well-conducting CSF layer covering the cortex, as shown by the iso-current density lines in this layer and their orientation perpendicular to this layer. (The direction of the current is

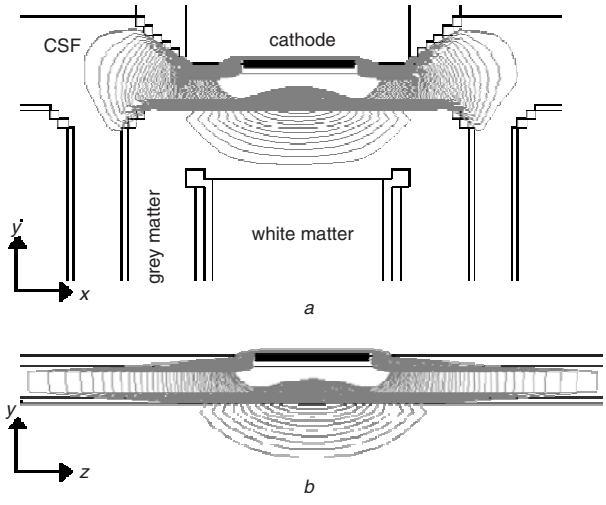

Fig. 5 *Iso-current density lines in (a) xy-plane and (b) yz-plane through the centre of cathode; 55 equidistant lines (5–60 μA mm^{-2}); monopolar cathodal stimulation (1 V)*

normal to the direction of the iso-current density lines.) Note that little current flows into the sulci. Efficacy calculations at both monopolar and bipolar stimulation in models with a 3.1 mm CSF layer thickness yielded that about 60% of the total cathodal current does not enter the cortex, but flows parallel to the electrode surface in the CSF layer. Below the electrode, the current also spreads approximately radially into the cortex, as shown in Figs 5*a* and *b*. The current densities in the cortex are, however, substantially lower than in the overlying CSF layer, as shown by the low values of the iso-current density lines (5–14 $\mu A\,mm^{-2}$).

Owing to its thickness (2 mm), the implantation of a lead for MCS will most probably reduce the thickness of the (highly conductive) CSF layer under the paddle. Because it is unknown how much the thickness of this layer will be reduced, we modelled several thicknesses to predict the effects on the current-density distribution and the load impedance in monopolar stimulation. If no CSF is present between the dura mater and the cortex under the lead paddle (Fig. 6, upper left plot), current penetrates deep into the cortex and the underlying white matter and enters the CSF on both sides of the paddle via the dura mater and the cortex. In this condition, the load impedance is high (975 Ω).

If a small CSF layer of 0.5 mm is present between the dura mater under the lead paddle and the cortex (Fig. 6, upper-right plot), the iso-current density lines penetrate less deeply into the white matter, indicating a reduced current density in the cortex and the underlying white matter. Moreover, the current density in the CSF on both sides of the paddle becomes higher, and the load impedance is reduced by ~20% compared with the model without CSF below the paddle. A further increase in the CSF layer thickness up to 2.5 mm results in a continued reduction in the current density in the cortex and white matter below the cathode and a further reduction in the load impedance, as shown in Fig. 6.

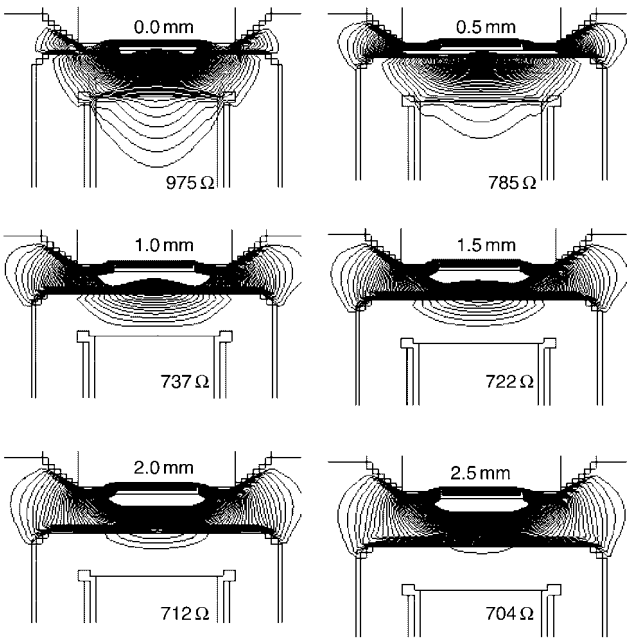

Fig. 6 *Iso-current density lines in the xy-plane through centre of cathode in six models having different thicknesses of CSF layer between electrode and cortex; 55 equidistant lines (5–60 $\mu A\,mm^{-2}$); monopolar cathodal stimulation (1 V); thickness of CSF layer and load impedance are indicated in each plot*

3.5 *Activating functions*

A first-order approximation of the effect of the stimulation-induced potential field on the membrane voltage of a nerve fibre is given by the activating function (AF), defined as the second-order difference of the nodal field potentials of a myelinated fibre (RATTAY, 1986). A positive AF indicates membrane depolarisation and possibly excitation, whereas a negative value indicates hyperpolarisation. The change in membrane potential increases with increasing value of AF.

AFs were calculated parallel to and perpendicular to the electrode surface, as shown in Fig. 7. The AFs were calculated along lines in the plotted model sections that coincide with the horizontal axes of the graphs. Fig. 7*a* shows the AF along a line in the *xy*-plane parallel to the cathodal surface at a depth of 1.4 mm in the cortex, for monopolar stimulation. The region in which the AF has a positive value is confined to a circular area under the cathode of about 6 mm (2 mm wider than the diameter of the cathode), and its maximum is located under the centre of the cathode.

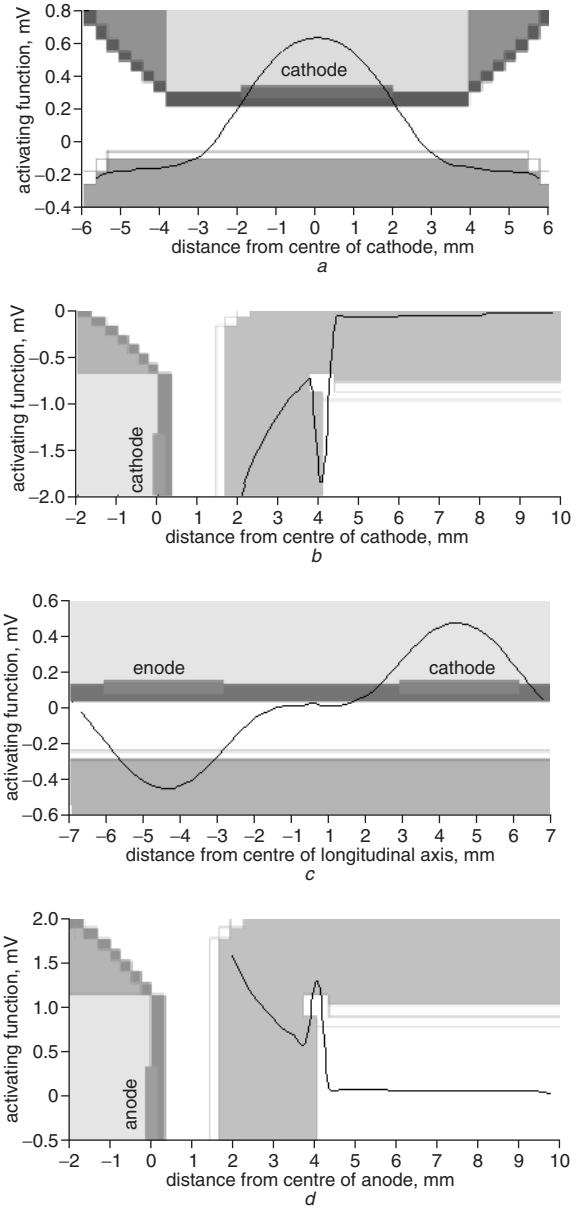

Fig. 7 *Activating functions along line in plotted model sections coinciding with the horizontal axis of each graph; (a), (b) monopolar cathodal stimulation (1 V); (c), (d) bipolar stimulation (1 V)*

Further from the cathode, the AF becomes slightly negative. Fig. 7*b* presents the AF along a line normal to the cathodal surface and crossing the centre of the cathode, for monopolar stimulation. Its value is most negative in layer I of the cortex and becomes almost zero in the underlying white matter. The sharp negative peak arises from the sudden change in electrical conductivity at the border of the cortex and the white matter.

At bipolar stimulation, the two cathodal AFs are identical to those at monopolar stimulation (shown in Figs 7*a*, and *b*), except for their slightly lower absolute values. Fig. 7*c* shows the AF along a line at a depth of 1.4 mm in the cortex and parallel to the line connecting the centres of the two electrodes. Its maximum and minimum are located under the centre of the cathode and the anode, respectively. In a region of ~3 mm centred between the electrodes, the AF value is almost zero. This means that the anodal and cathodal fields hardly overlap, and that the anode and cathode can be considered as virtual monopoles (see also Section 3.2). The two anodal AFs are mirror images of the cathodal ones: being positive and negative along a line normal and parallel to the anodal surface, respectively (see Figs 7*c* and *d*).

The AF curves in Figs 7*c* and *d* were calculated in a bipolar stimulation model that was calibrated at a ~200 Ω higher load impedance than the monopolar model (see Section 2.1.2). Because the same voltage was applied between cathode and anode in both models (the model boundary being the anode in monopolar stimulation), the current density near the cathode was higher in the monopolar case. Consequently, monopolar voltage-controlled stimulation results in somewhat higher potential gradients and higher absolute AF values than bipolar stimulation.

3.6 *Threshold stimuli for fibre excitation*

The threshold stimuli of the fibre types shown in Fig. 3 were calculated for monopolar (cathodal), voltage-controlled stimulation with monophasic pulses of 0.21 ms duration. Under these stimulation conditions, efferent fibres of type E_1 were hyperpolarised, which is in accordance with the negative AF values calculated in the preceding Section (only fibres with a direction component parallel to the electrode surface are excitable by a cathode).

Fig. 8 shows the normalised threshold stimuli of the fibre types E_2, E_3 and A_1 as a function of their diameter (5–15 μm). As shown by the shape of the curves, the threshold amplitudes of the three fibre types have a similar dependence on their diameter. Efferent fibre type E_2 (with an initial angle of 45° to the electrode surface) has the highest threshold.

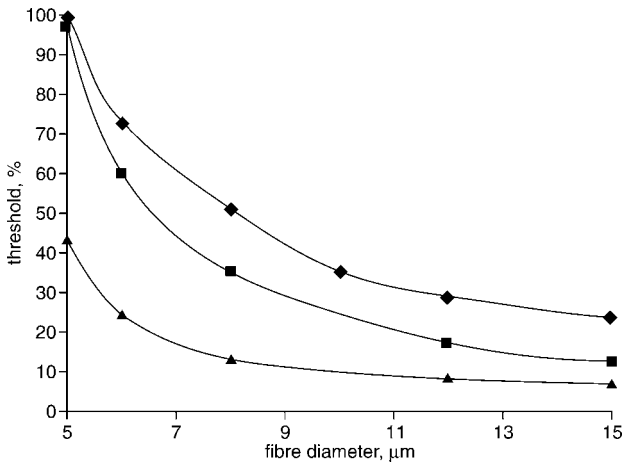

Fig. 8 *Normalised threshold voltages of cathodally excitable fibre types ((-▲-) A_1, (-◆-) E_2, (-■-) E_3) as function of their diameter (5–15 μm) in monopolar stimulation*

Although further away from the electrode, efferent fibre type E_3 has a lower threshold, which should be attributed to its initial orientation parallel to the cathodal surface. Fibre type A_1 has the lowest threshold, probably because it is nearest to the cathode and oriented parallel to the electrode surface. Note that the thresholds were calculated for simple fibre models (see Section 4) and that they will probably be different when more realistic fibre models are applied.

The excitation threshold of a 5 μm type A_1 fibre was calculated in models with each of the six CSF layer thicknesses depicted in Fig. 6. A linear fit of the data points ($R^2 = 0.97$) yielded a sensitivity of 6.6 $V_{threshold}$ mm^{-1} CSF. The excitation threshold of the type A_1 fibre varied also linearly with its depth in the cortex ($R^2 = 1$), yielding a sensitivity of 3.3 $V_{threshold}$ mm^{-1} depth.

In bipolar voltage-controlled stimulation at a pulsewidth of 0.21 ms, the threshold curves have the same shape as in monopolar stimulation. Owing to a 33% higher load impedance of the bipolar model, the threshold voltages are proportionately higher. When fibre type E_1 was placed below the centre of the anode, it could be excited, in contrast to the situation when it was placed under the cathode. Moreover, its threshold stimulus was lower than for fibre types E_2 and E_3 with the same diameter placed under the cathode.

4 Discussion

4.1 *Volume conductor model*

As the compartments filled with CSF have a much higher electrical conductivity than the other anatomical compartments of the model (see Table 2), their geometry may be a critical factor. In contrast to the width of the sulci, which hardly affects the current-density field in the cortex below an electrode, this field is affected substantially by variation in the thickness of the CSF layer between the cortex and the dura mater under the electrode. In our standard model, the thickness of the resume lead paddle (2 mm) was subtracted from the (mean) CSF layer thickness (3.1 mm). As no imaging data are yet available on the thickness of the CSF layer and the shape of the cortex below the implanted lead paddle, improvements in modelling MCS should be focused primarily on these anatomical aspects.

4.2 *Nerve fibre models*

4.2.1 *Efferent fibres:*

All fibre types modelled in this study were represented by a simple, straight or curved, myelinated nerve fibre model. In reality, a nerve fibre originates from a neuronal cell body having dendritic extensions as well. A complete neuron model would be most appropriate to simulate the electrical behaviour of pyramidal cells in the precentral cortex. Nevertheless, even with our simple efferent fibre models E_1, E_2 and E_3, an initial comparative guess of threshold stimuli can be obtained.

Because in neocortical cells the time constant of the soma-dendritic membrane (15 ± 7 ms) is generally more than 160-fold the time constant of the nodal membrane (Nowak and Bullier, 1998), a short stimulation pulse (0.1–0.2 ms) just exciting a myelinated fibre will hardly affect the soma-dendritic membrane potential of the same neuron.

Empirical studies have confirmed that axons are the targets of external stimulation of brain tissue (Porter, 1963; Nowak and Bullier, 1998). Computer modelling of a complete neuron has shown that action potentials were initiated neither at the soma nor in dendritic tree branches, but always at (the initial segment of) the axon, irrespective of the stimulus

polarity and the orientation of the neuron in the extracellular field (RATTAY, 1999). To yield a proper estimate of the threshold stimulus when using a simple efferent fibre model, the termination impedance at its proximal end should equal the input impedance of the missing soma-dendritic part of the neuron.

4.2.2 *Afferent fibres*

The type A_1 afferent fibre has been modelled as a simple 'horizontal' fibre at a depth of 1.4 mm in the cortex. In reality, on leaving the white matter, afferents ascend normal to the laminated structure of the cortex up to a layer where they bifurcate. The fibre branches extend within this layer and make en-passage synaptic contacts with local cortical neurons. In a modelling study on the recruitment of dorsal column fibres in the spinal cord, it has been shown that the presence of collaterals normal to the dorsal column fibre (radial to the cathode) reduce the threshold stimulus by up to 50% compared with an unbranched fibre (STRUIJK *et al.*, 1992). As a similar geometrical situation would exist when a cortical afferent was modelled as a branched fibre, its threshold stimulus would be reduced substantially compared with the value of the simple A_1 fibre model we used.

4.2.3 *Fibre diameters*

Another crucial aspect in the comparison of threshold stimuli of different fibre types in the motor cortex is the maximum of their diameter distributions, which determines the threshold stimulus of each fibre type. However, data about fibre calibres of afferents and efferents in the various layers of the human primary motor cortex are still missing.

The goal of this initial modelling study was to develop an MCS model and test the influence of certain model parameters on the imposed electrical potential field. The further development of this model will primarily be focused on more sophisticated fibre models with realistic diameters, to allow improved prediction of their recruitment.

4.3 *Empirical and modelled stimulation amplitude data*

MCS is generally applied bipolarly, with the cathode over the cortical region corresponding to the painful body area (NGUYEN *et al.*, 1999; TSUBOKAWA *et al.*, 1993) at an amplitude ranging from 2 to 8 V (SMITH *et al.*, 2001). Taking into account the high sensitivity of the stimulation threshold of cortical fibres to the thickness of the overlying CSF layer (6.6 V mm^{-1} CSF for fibre type A_1), such a wide range is likely to occur, particularly when the effects of other variables, such as the pulsewidth (0.06–0.5 ms (SMITH *et al.*, 2001)) and the percentage of the motor threshold voltage chosen as the chronic stimulation level (20–50%) are considered as well. These variables prevent a meaningful comparison of empirical and calculated stimulation voltages.

The low threshold for excitation of the efferent type E_1 fibre under the anode, as predicted by modelling, is consistent with empirical studies reporting that *anodal* stimulation on the convexity of the precentral gyrus directly activates cortical efferents at a lower stimulus amplitude than *cathodal* stimulation does (GORMAN, 1966; HERN *et al.*, 1962; PHILLIPS and PORTER, 1962).

The diameter of Betz cells varies from ~60 to ~120 μm, with the smallest cells located in the inferior part of the precentral gyrus, and the largest ones located in the superior part (TRUEX and CARPENTER, 1964). Under the assumption that the axon diameter is correlated with the size of the cell body, the motor threshold would be higher for stimulation of the facial area than, for example, a limb area. However, no empirical data are yet available to test this hypothesis.

4.4 *Cortical fibres most likely to mediate the analgesic effect of MCS*

As it has been shown by brain imaging that the thalamic VA–VL complex is activated by MCS (GARCIA-LARREA *et al.* (1999)), cortical nerve fibres most probably mediating the analgesic effect are either cortico-thalamic fibres or thalamo-cortical fibres, the latter by antidromic propagation of the stimulation-induced action potentials towards the collateral fibre terminals in these thalamic nuclei.

In clinical practice, MCS is applied cathodally at 20–50% of the motor threshold. This motor threshold is most probably related to the stimulation of large type E_2 or type E_3 corticospinal fibres arising from Betz cells in layer V. Because these fibres have a larger diameter than cortico-thalamic fibres arising in layers V and VI, it is unlikely that the latter are *directly* activated and induce the analgesic effect at a stimulation amplitude 50–80% below the threshold of motor responses. Future modelling work should provide an answer to this question.

5 Conclusions

The thickness of the CSF layer between the dura mater and the cortex below the cathode affects the threshold amplitude for motor responses and the therapeutic stimulation amplitude in MCS substantially.

Owing to the large centre-to-centre distance of the electrodes currently applied in MCS, the anodal and cathodal fields hardly interfere in bipolar stimulation. Accordingly, there will be virtually no difference between the responses to monopolar (cathodal) and bipolar stimulation, except for a higher voltage (and energy) needed in bipolar stimulation.

Bipolar stimulation with the anode placed over the superior region of the precentral gyrus should be avoided, as cortical efferents in the convexity of the gyrus have a low threshold when stimulated by an anode. The anode should thus not be considered an indifferent (inactive) electrode contact. Both cathode and anode position can be relevant to the clinical effects of MCS.

Acknowledgments—The authors are grateful to Dr Kees Venner (Mechanical Engineering Deptartment, University of Twente, The Netherlands) for his valuable advice on numerical algorithms.

References

BROWN, J. A., and BARBARO, N. M. (2003): 'Motor cortex stimulation for central and neuropathic pain: current status', *Pain*, **104**, pp. 431–435

GARCIA-LARREA, L., PEYRON, R., MERTENS, P., GREGOIRE, M. C., LAVENNE, F., LE BARS, D., CONVERS, P., MAUGUIÈRE, F., SINDOU, M., and LAURENT, B. (1999): 'Electrical stimulation of motor cortex for pain control: a combined PET-scan and electrophysiological study', *Pain*, **83**, pp. 259–273

GORMAN, A. L. F. (1966): 'Differential patterns of activation of the pyramidal system elicited by surface anodal and cathodal cortical stimulation', *J. Neurophysiol.*, **29**, pp. 547–564

GRAF VON KEYSERLINGK, D., and SCHRAM, U. (1984): 'Diameter of axons and thickness of myelin sheaths of pyramidal tract fibres in the adult human medullary pyramid', *Anat. Anz.*, **157**, pp. 97–111

HABERLY, L. B., and SHEPHERD, G. M. (1973): 'Current-density analysis of summed evoked potentials in Opossum prepyriform cortex', *J. Neurophysiol.*, **36**, pp. 789–803

HERN, E. C., LANDGREN, S., PHILLIPS, C. G., and PORTER, R. (1962): 'Selective excitation of corticofugal neurones by surface anodal stimulation of the Baboon's motor cortex', *J. Physiol. (London)*, **161**, pp. 73–90

HOELTZELL, P. B., and DYKES, R. W. (1979): 'Conductivity in the somatosensory cortex of the cat: evidence for cortical anisotropy', *Brain Res.*, **177**, pp. 61–82
JIANG, D. F. (1990): 'Study of some morphologic aspects of the human dura mater', *Chin. J. Surg.*, **28**, pp. 108–109, p. 128
MCCOMB, J. G., WITHERS, G. J., and DAVIS, R. L. (1981): 'Cortical damage from Zenker's solution applied to the dura mater', *Neurosurg.*, **8**, pp. 68–71
MCNEAL, D. R. (1976): 'Analysis of a model for excitation of myelinated nerve', *IEEE Trans. Biomed. Eng.*, **23**, pp. 329–337
NA, J., KAKEI, S., and SHINODA, Y. (1997): 'Cerebellar input to corticothalamic neurons in layers V and VI in the motor cortex', *Neurosci. Res.*, **28**, pp. 77–91
NGUYEN, J.-P., LEFAUCHEUR, J.-P., DECQ, P., UCHIYAMA, T., CARPENTIER, A., FONTAINE, D., BRUGIÈRES, P., POLLIN, B., FÈVE, A., ROSTAING, S., CESARO, P., and KERAVEL, Y. (1999): 'Chronic motor cortex stimulation in the treatment of central and neurophatic pain. Correlations between clinical, electrophysiological and anatomical data', *Pain*, **82**, pp. 245–251
NGUYEN, J. P., LEFAUCHEUR, J. P., LE GUERINEL, C., EIZENBAUM, J. F., NAKANO, N., CARPENTIER, A., BRUGIERES, P., POLLIN, B., ROSTAING, S., and KERAVEL, Y. (2000): 'Motor cortex stimulation in the treatment of central and neuropathic pain', *Arch. Med. Res.*, **31**, pp. 263–265
NIEUWENHUYS, R., VOOGD, J., and VAN HUIJZEN, C. (1988): 'The human central nervous system. A synopsis and atlas, 3rd edn' (Springer Verlag, Berlin, 1988)
NOWAK, L. G., and BULLIER, J. (1998): 'Axons, but not cell bodies, are activated by electrical in cortical gray matter', *Exp. Brain Res.*, **118**, pp. 477–488
OHYE, C. (1990): 'Thalamus', in PAXINOS, G. (Ed.): 'The human nervous system' (Academic Press, San Diego, New York, 1990), Chap. 17, pp. 439–468
PHILLIPS, C. G., and PORTER, R. (1962): 'Unifocal and bifocal stimulation of the motor cortex', *J. Physiol. (London)*, **162**, pp. 532–538
PIROTTE, B., VOORDECKER, P., JOFFROY, F., MASSAGER, N., WIKLER, D., BALERIAUX, D., LEVIVIER, M., and BROTCHI, J. (2001): 'The Zeiss-MKM system for frameless image-guided approach in epidural motor cortex stimulation for central neuropathic pain', *Neurosurg. Focus*, **11**, (3): Article 3, pp. 1–6
PORTER, R. (1963): 'Focal stimulation of hypoglossal neurones in the cat', *J. Physiol. (London)*, **169**, pp. 630–640
RATTAY, F. (1986): 'Analysis of models for external stimulation of axons', *IEEE Trans. Biomed. Eng.*, **33**, pp. 974–977
RATTAY, F. (1999): 'The basic mechanism for the electrical stimulation of the nervous system', *Neurosci.*, **2**, pp. 335–346
SMITH, H., JOINT, C., SCHLUGMAN, D., NANDI, D., STEIN, J., and AZIZ, T. Z. (2001): 'Motor cortex stimulation for neuropathic pain', *Neurosurg. Focus*, **11**, (3): Article 2, pp. 1–9
STRUIJK, J. J., HOLSHEIMER, J., VAN DER HEIDE, G. G., and BOOM, H. B. K. (1992): 'Recruitment of dorsal column fibers in spinal cord stimulation: Influence of collateral branching', *IEEE Trans. Biomed. Eng.*, **39**, pp. 903–912
TANG, Y., and NYENGAARD, J. R. (1997): 'A stereological method for estimating the total length and size of myelin fibers in human brain white matter', *J. Neurosci. Methods*, **73**, pp. 193–200.
TRUEX, R. C., and CARPENTER, M. B. (1964): 'Human anatomy' (The Williams & Wilkins Company, Baltimore, 1964)
TSUBOKAWA, T., KATAYAMA, Y., YAMAMOTO, T., HIRAYAMA, T., and KOYAMA, S. (1993): 'Chronic motor cortex stimulation in patients with thalamic pain', *J. Neurosurg.*, **78**, pp. 393–401
VILLIGER, L. (1940): 'Gehirn und Rückenmark' (Wilhelm Engelmann Verlag, Leipzig, 1940)
WESSELINK, W. A., HOLSHEIMER, J., and BOOM, H. B. K. (1999): 'A model of the electrical behaviour of myelinated sensory nerve fibres based on human data', *Med. Biol. Eng. Comput.*, **37**, pp. 228–235
ZEFFIRO, T. A. (1990): 'Motor cortex', in PAXIONS, G. (Ed.): 'The human nervous system' (Academic Press, San Diego, New York 1990), Chap. 23, pp. 803–810
ZILLES, K. (1990): 'Cortex', in PAXIONS, G. (Ed.): 'The human nervous system' (Academic Press, San Diego, New York, 1990), Chap. 22, pp. 757–802

Authors' biographies

LJUBOMIR MANOLA was born in Belgrade, Serbia, in 1977. In 2002, he graduated from the Department of Electronics, Faculty of Electrical Engineering, University of Belgrade. In the same year, he joined the Institute for Biomedical Technology, University of Twente, The Netherlands, where he is pursuing a PhD degree. His research comprises computer modelling of clinical neuromodulation techniques, such as electrical spinal cord and motor cortex stimulation in the management of chronic, otherwise intractable pain. His research includes the exploration of ways to manipulate the primary effects of stimulation on nerve tissue.

BAS ROELOFSEN was born in Rhenen, The Netherlands, in 1978. He studied Electrical Engineering at the University of Twente, The Netherlands, where he fulfilled his Masters assignment at the Institute for Biomedical Technology. He developed a computer model for the simulation of motor cortex stimulation in the management of chronic pain, based on human anatomical data. He received his MSc degree in 2003 and he is currently working in industry as a Software Engineer.